Interaction of cationic, anionic and non-ionic macroRAFT homo and copolymers with Laponite clay

SUPPORTING INFORMATION

1) Adsorption isotherm models

The adsorption models used to fit the experimental data are displayed in Table S1.

Table S1 Equilibrium adsorption models employed to fit the experimental data.

Model	Equation	Eq.
Langmuir	$q_e = q_{max,L}\frac{K_L C_e}{1 + K_L C_e}$	S1
Freundlich	$q_e = K_F C_e^{\frac{1}{n_F}}$	S2
Tempkin	$q_e = \frac{RT}{b_T}\ln A_T C_e$	S3
Sips	$q_e = q_{max,S}\frac{K_S C_e^{\frac{1}{n_S}}}{1 + K_S C_e^{\frac{1}{n_S}}}$	S4
Redlich-Peterson	$q_e = q_{max,RP}\frac{K_{RP} C_e}{1 + K_{RP} C_e^{\beta}}$	S5
BET	$q_e = q_{max,B}\frac{K_{B1} C_e}{(1 - K_{B2} C_e)(1 - K_{B2} C_e + K_{B1} C_e)}$	S6

The Langmuir and Freundlich isotherms apply over a wide concentration range and thus these are the most commonly used models to fit adsorption isotherm data. Langmuir isotherm[1] is a two-parameter model, characterized graphically by a plateau that corresponds to saturation equilibrium. It assumes monolayer adsorption, so, after the saturation plateau is achieved, no more adsorption takes place and the solid has reached its maximum adsorption capacity, $q_{max,L}$ (eq. S1). It also assumes that the adsorbent has a homogeneous surface and, therefore, all adsorption sites are associated to equal heat of adsorption. Even though these two assumptions can be reasonable for the adsorption of organic molecules onto solid surfaces in liquid solution, the model was originally developed for the adsorption of gas molecules, therefore it does not predict solute-solute or solute-solvent interactions, and it considers that solute and solvent have similar molar surface area. In the Langmuir expression, K_L is a Langmuir constant, C_e is the adsorbate concentration in the liquid phase and q_e is its concentration in the solid phase at equilibrium. The Freundlich isotherm[2] (eq. S2) is an exponential equation so, contrary to Langmuir, a plateau is not reached and, theoretically, the concentration of adsorbate on the solid surface can increase until infinite adsorption. It can be applied to multilayer, non-ideal and reversible adsorption over heterogeneous surfaces. The empirical model is characterized by Freundlich constants K_F, which can be related to the adsorption capacity, and n_F, the heterogeneity factor, which can be related to the surface heterogeneity or the adsorption intensity (energy of adsorption). In the Tempkin adsorption model (eq. S3), the effect of adsorbate/adsorbate interactions is considered and the heat of adsorption of all molecules in the layer is assumed to decrease linearly with increasing the coverage due to these interactions. The constant B ($B=RT/b_T$) is related to the heat of adsorption, while

A_T is related to the maximum binding energy. The Sips model[3] is a three-parameter equation (eq. S4) that generalizes Langmuir and Freundlich models. The equation approaches the Freundlich model at low concentrations of adsorbate and the Langmuir model at high concentrations, predicting a monolayer adsorption capacity. Similarly, the Redlich-Peterson isotherm[4] (eq. S5) associates Langmuir and Freundlich models into a three-parameter equation but, contrarily to Sips; it approaches the Langmuir model at low concentrations of adsorbate (following Henry's law) and the Freundlich model at high concentrations. In fact, the value of the exponent β lies between 0 and 1 and, when β=1, the model reduces to Langmuir equation. The Brunauer-Emmett-Teller isotherm[5] (eq. S6) is a sole theoretical model that comprises three parameters. Developed for adsorption of gas on solid, this model describes multilayer adsorption by successively applying the Langmuir equation to each layer and assuming that the heat of adsorption of the first layer is different from that of all subsequent layers. The correct form of this equation is given in eq. S6,[6] where $q_{max,B}$ is the monolayer adsorption capacity, K_{B1} is the adsorption equilibrium constant of the first layer and K_{B2} is the adsorption equilibrium constant of the upper layers.

For the determination of the constants of each model, the equations displayed in Table S1 were adjusted to the experimental data and the Solver add-in of Microsoft Excel® was used to minimize the hybrid functional error function (HYBRID, developed to improve the fit of the sum of the squares of the errors at low concentrations), as shown in Eq. S7:

$$HYBRID = \frac{100}{p-n}\sum_{i=1}^{p}\left[\frac{(q_{e,exp}-q_{e,model})_i^2}{q_{e,exp}}\right]_i \qquad \text{(S7)}$$

Where p is the number of data points and n is the number of constants of the adsorption isotherm model. $q_{e,exp}$ is the amount of macroRAFT agent adsorbed on the clay at equilibrium determined experimentally, while $q_{e,model}$ is the theoretical amount determined using the models. The quality of the fit of the model was evaluated by calculating the coefficient of determination (R^2).

2) Synthesis of macroRAFT agents

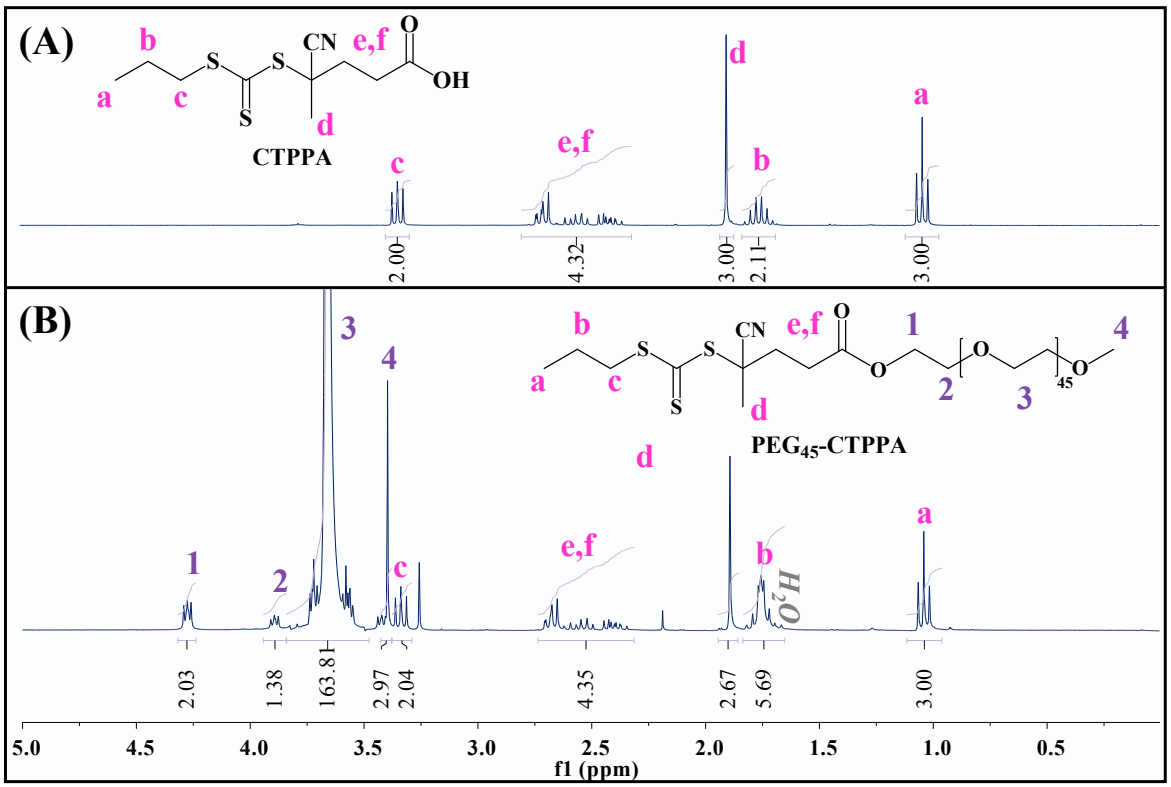

Figure S1. ^{1}H NMR spectra of (A) CTPPA and (B) PEG_{45}-CTPPA macroRAFT agent (MR3) synthesized via an esterification reaction between mPEG (2000 g mol^{-1}) and

CTPPA. The comparison between both spectra indicates that PEG_{45}-CTPPA with a high degree of purity was obtained.

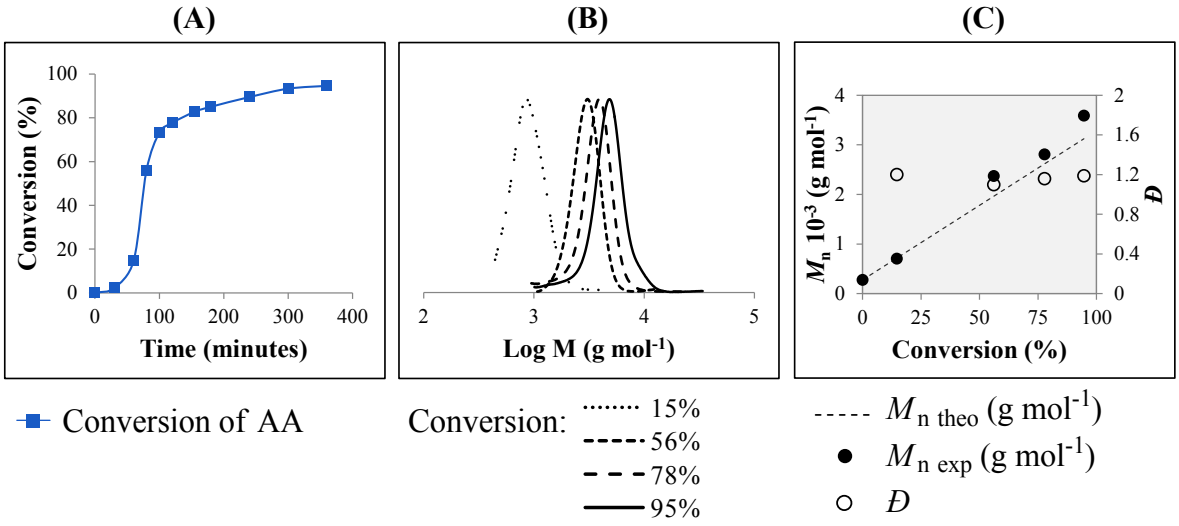

Figure S2. RAFT polymerization of AA in 1,4-dioxane at 80°C. (A) Evolution of AA conversion versus time, determined by ^{1}H NMR; (B) THF-SEC chromatogram peaks and (C) number-average molar masses (M_n, full symbols) and dispersities ($Đ$, open symbols) with overall monomer conversion for the synthesis of PAA_{40}-CTPPA (MR1). For the determination of M_n and $Đ$, the product was purified and methylated before analysis.

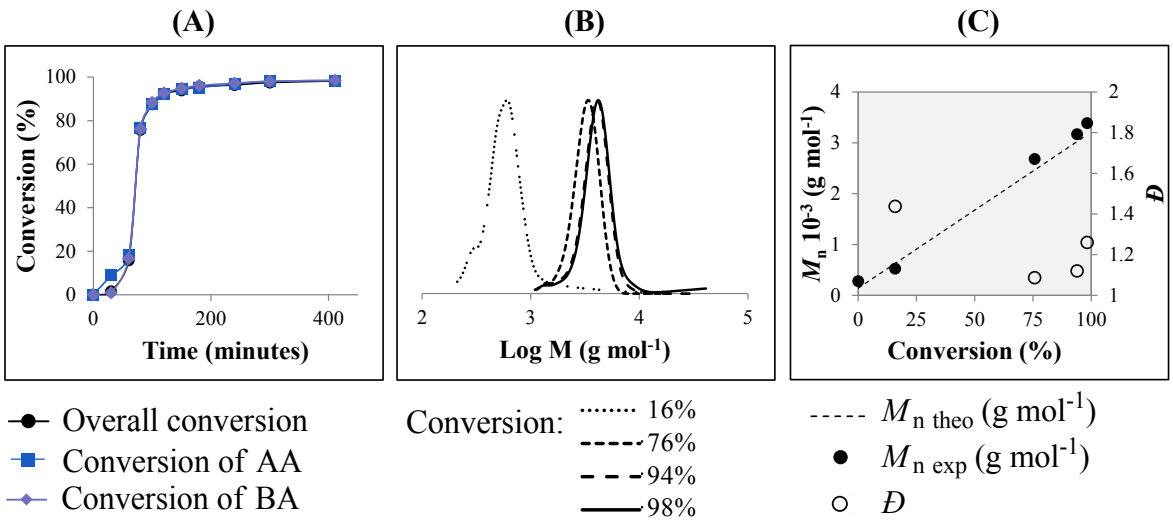

Figure S3. RAFT copolymerization of AA with BA in 1,4-dioxane at 80°C. (A) Evolution of monomer conversion with time; (B) size exclusion chromatogram peaks and (C) evolution of the number-average molar masses (M_n, full symbols) and dispersities ($Đ$, open symbols) with monomer conversion, determined by SEC in THF, for the synthesis of P(AA_{16}-*co*-BA_{16})-CTPPA (MR2). As the polymers were not purified after methylation, it can be speculated that the high dispersity obtained at the beginning of polymerization is due to the superposition of the peak from the sample with the signal from the methylation agent, since a low molar mass (560 g mol^{-1}) was reached until this point.

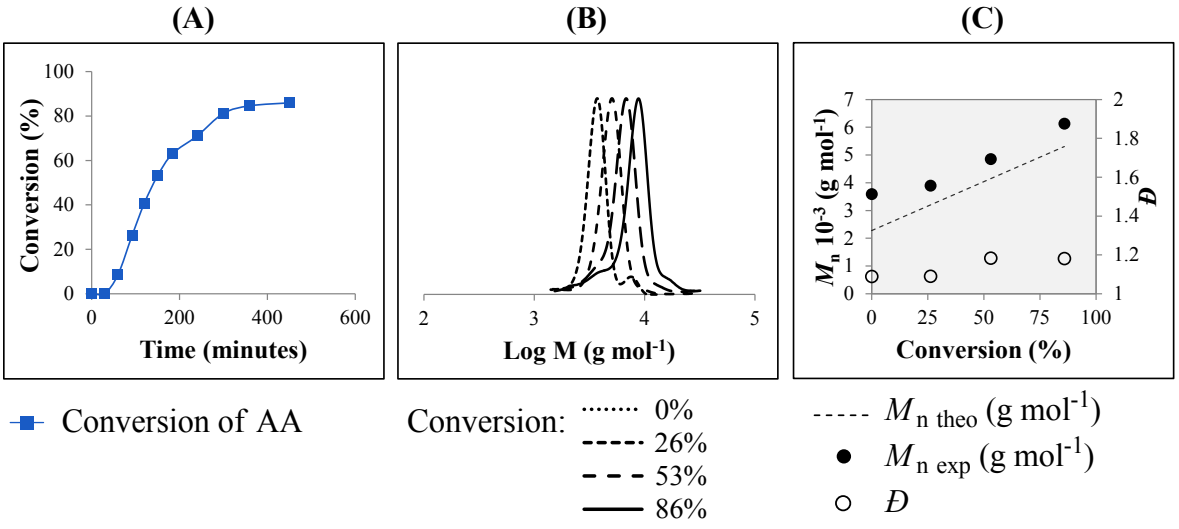

Figure S4. RAFT polymerization of AA in 1,4-dioxane at 80°C using PEG_{45}-CTPPA as chain transfer agent. (A) Evolution of AA conversion, determined by ^1H NMR, versus time; (B) THF-SEC chromatogram peaks and (C) number-average molar masses (M_n, full symbols) and dispersities ($Đ$, open symbols) with overall monomer conversion for the synthesis of PEG_{45}-*b*-PAA_{42}-CTPPA (MR4). The small shoulder on the low molar mass side of the chromatograms can be likely attributed to remaining PEG_{45}-CTPPA chains that were not activated or to residual mPEG from the synthesis of PEG_{45}-CTPPA. The precursor curve presents a peak of lower intensity that could be attributed to the existence of chains with higher molar mass in commercial mPEG or to coupling reactions between some PEG_{45}-CTPPA molecules. Even though the data showed a linear behavior, confirming the living character of AA polymerization in the presence of PEG_{45}-CTPPA, they did not follow the theoretical curve, from which they are deviating

of approximately 1300 g mol^{-1} due to the use of PMMA standards, which are not the most indicated for PEG chains.

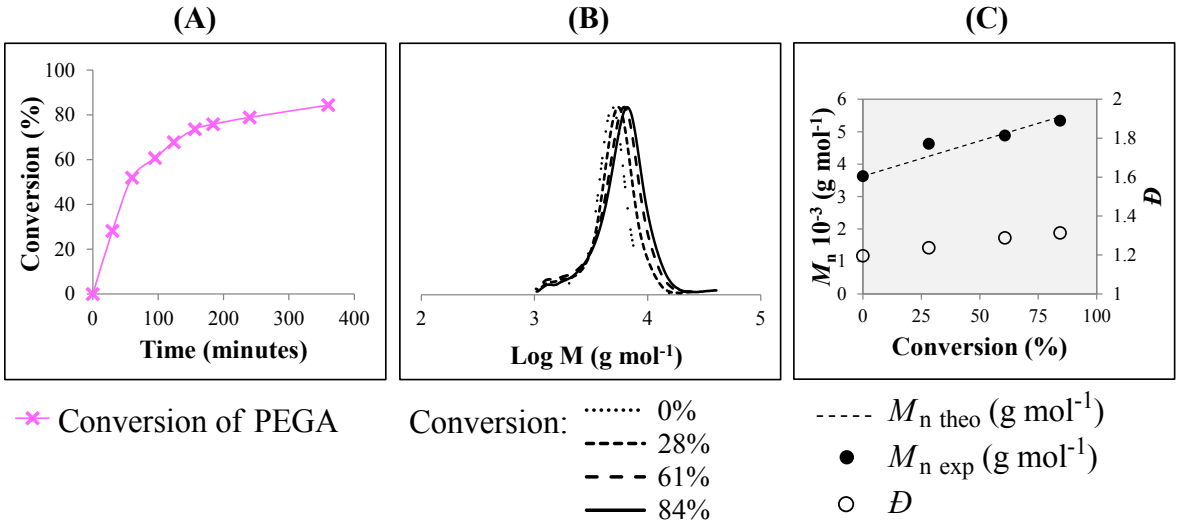

Figure S5. RAFT polymerization of PEGA in 1,4-dioxane at 80°C using PAA_{40}-CTPPA (MR1) as chain transfer agent. (A) Evolution of PEGA conversion, determined by ^{1}H NMR, versus time; (B) THF-SEC chromatogram peaks and (C) number-average molar masses (M_n, full symbols) and dispersities ($Đ$, open symbols) with overall monomer conversion for the synthesis of PAA_{40}-*b*-$P(PEGA_4)$-CTPPA (MR5).

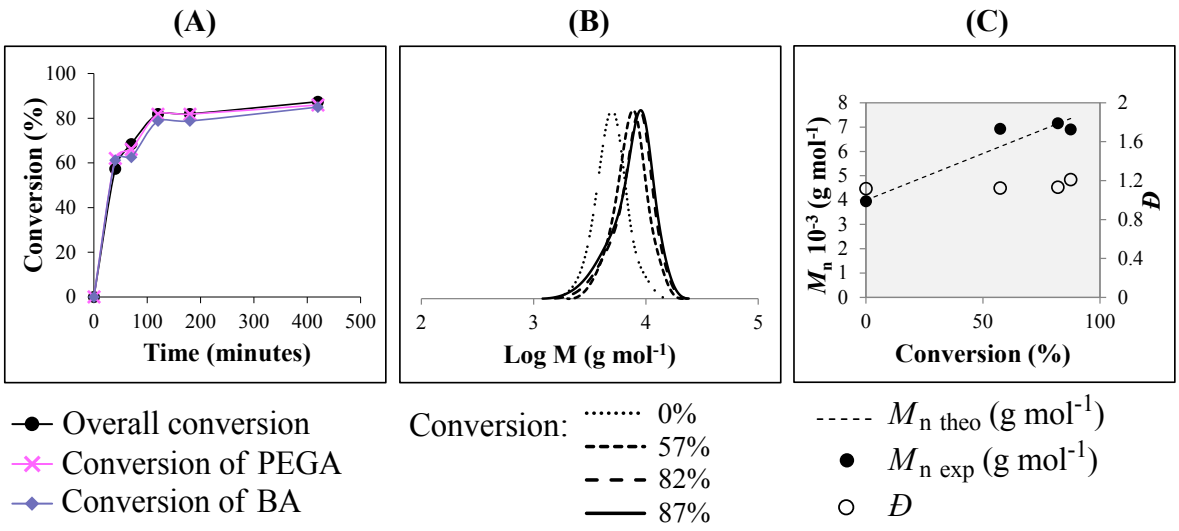

Figure S6. RAFT polymerization of PEGA in 1,4-dioxane at 80°C using macroRAFT agent PAA_{40}-CTPPA (MR1) as chain transfer agent. (A) Evolution of PEGA conversion, determined by ^1H NMR, versus time; (B) THF-SEC chromatogram peaks and (C) number-average molar masses (M_n, full symbols) and dispersities ($Đ$, open symbols) with overall monomer conversion for the synthesis of PAA_{40}-*b*-P($PEGA_6$-*co*-BA_4)-CTPPA (MR7). Individual conversions were similar for both monomers, which indicates the absence of composition drift, however, the remaining shoulder might indicate that some of the chains from the precursor were not activated and did not suffer chain extension with PEGA and BA.

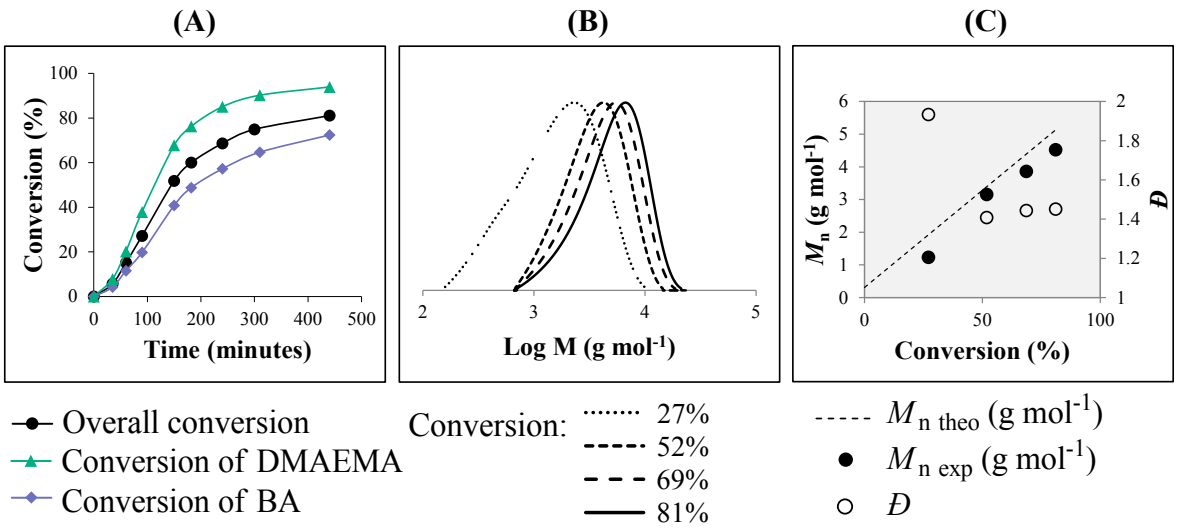

Figure S7. RAFT copolymerization of DMAEMA and BA in solution of 1,4-dioxane at 80°C. (A) Evolution of monomer conversion with time, with DMAEMA individual conversion higher than BA during all polymerization; (B) size exclusion chromatogram peaks and (C) evolution of the number-average molar masses (M_n; full symbols) and dispersities ($Đ$; open symbols) with monomer conversion, for the synthesis of P(DMAEMA$_{19}$-*co*-BA$_{14}$)-CTPPA (MR11). The product was characterized by SEC using PMMA standards and THF with lithium bromide as eluent.

3) Constants estimated for adsorption models of non-ionic, anionic and cationic macroRAFT agents onto Laponite

Table S2. Langmuir, Freundlich and Tempkin constants estimated by nonlinear regression for the adsorption of non-ionic, anionic and cationic macroRAFT agents. Laponite concentration = 5.0 g L^{-1}.

Macro RAFT	Langmuir				Freundlich			Tempkin*		
	$q_{max,L}$ (mg g^{-1})	K_L (L mg^{-1})	K_D (L g^{-1})	R^2	K_F (L mg^{-1})	n_F (L mg^{-1})	R^2	B	A	R^2
MR1	18	6.02	109	0.9456	11	0.36	0.9464	3	562	0.8858
MR2	320	0.31	100	0.9885	72	0.71	0.9923	28	40	0.7669
MR3	470	3.27	1536	0.9107	282	0.26	0.9729	72	81	0.9779
MR4	173	1.07	186	0.9759	93	0.24	0.9121	31	17	0.9608
MR5	453	0.22	101	0.9987	96	0.50	0.9798	81	3	0.9703
MR6	466	2.26	1053	0.9693	287	0.34	0.8701	239	5	0.6241
MR7	488	0.74	361	0.9849	217	0.32	0.8531	107	7	0.9510
MR8	208	0.89	184	0.9592	93	0.41	0.9847	24	140	0.8723
MR9	534	0.19	104	0.9657	87	0.68	0.9436	78	5	0.8821
MR10q	2351	0.45	1050	0.8957	1024	0.22	0.9038	165	1274	0.7944
MR11q	1426	7.98	11384	0.7732	1435	0.41	0.7718	300	80	0.7805
MR11	876	53.94	47239	0.7898	692	0.14	0.7724	93	3044	0.8416

*B = RT/b

Table S3. Redlich-Peterson, Sips and BET constants estimated by nonlinear regression for the adsorption of non-ionic, anionic and cationic macroRAFT agents. Laponite concentration = 5.0 g L^{-1}.

Macro RAFT	Redlich-Peterson				Sips				BET			
	$q_{max,RP}$ (mg g^{-1})	K_{RP}	N_{RP}	R^2	$q_{max,S}$ (mg g^{-1})	K_S (L mg^{-1})	n_S (L mg^{-1})	R^2	$q_{max,B}$ (mg g^{-1})	K_{B1} (L mg^{-1})	K_{B2} (L mg^{-1})	R^2
MR1	14	15.3	0.81	0.9967	24	1.16	1.459	0.9964	14	13.9	0.051	0.9971
MR2	73	46.9	0.30	0.9980	12297	0.01	1.404	0.9980	104	1.4	0.134	0.9980
MR3	336	12.4	0.83	0.9983	604	1.08	1.734	0.9923	375	6.0	0.021	0.9967
MR4	152	1.5	0.95	0.9928	184	0.95	1.173	0.9925	160	1.3	0.006	0.9936
MR5	315	0.4	0.97	0.9998	514	0.20	1.127	0.9998	381	0.3	0.007	0.9998
MR6	651	1.1	1.25	0.9968	411	5.52	0.604	0.9985	466	2.3	0.000	0.9936
MR7	698	0.4	1.16	0.9994	438	0.92	0.757	0.9998	488	0.7	0.000	0.9985
MR8	516	0.2	1.51	0.9971	197	1.00	0.899	0.9934	208	0.9	0.000	0.9920
MR9	136	1.5	0.43	0.9844	742	0.13	1.152	0.9892	534	0.2	0.000	0.9906
MR10q	1024	1.08E+10	0.78	0.9744	311913	0.00	3.333	0.9825	1116	5.7	0.038	0.9702
MR11q	1460	9.9	0.86	0.9449	1750	3.09	1.298	0.9450	1198	10.2	0.167	0.9450
MR11	791	90.4	0.94	0.9264	853	620.25	0.948	0.8781	755	72.8	0.016	0.9244

4) Control over the macroRAFT/Laponite initial dispersion of MR10q and MR11

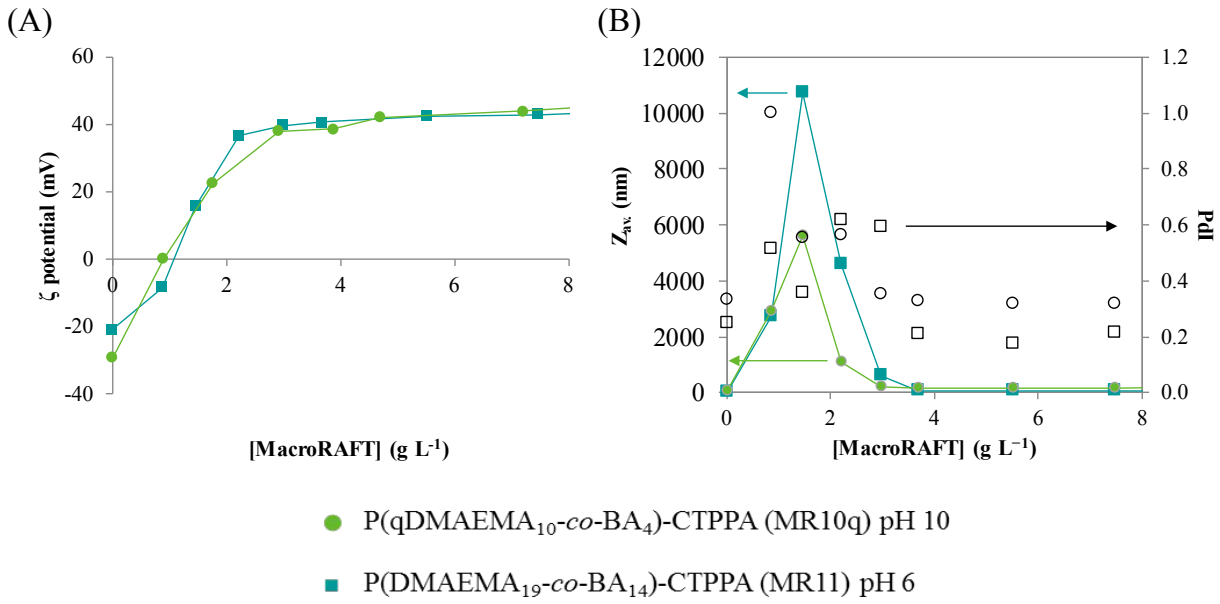

Figure S8. Evolution of (A) ζ potential and (B) average hydrodynamic diameters (full symbol) and PdI (empty symbol) of Laponite platelets functionalized with different concentrations of MR10q at pH 10 and MR11 at pH 6. [Laponite] = 5 g L^{-1}.

5) X-ray diffraction analysis

X-Ray diffraction (XRD) analysis were carried out in the *Laboratório de Caracterização Tecnológica* (*Depto. de Engenharia de Minas e de Petróleo*) from *Escola Politécnica da USP*, São Paulo, Brazil. Powder X-ray diffraction data were collected on a Bruker D8 Endeavor diffractometer operating at 40 kV and 40 mA for Cu Kα (λ = 1.54056 Å), with

a scan speed of 0.5s per step and a step size of 0.02 ° in 2θ. The angular domain analyzed was comprised between 1.5 and 75 °.

Four samples were prepared by initially dispersing 0.9 g of Laponite into 45 mL of water. The dispersion was left under vigorous stirring while a solution of macroRAFT agent was prepared in parallel by adding 0.51 g of macroRAFT agent P(DMAEMA$_{19}$-*co*-BA$_{14}$)-CTPPA and 17g of water into a 30 mL flask. The solution was left stirring and had its pH adjusted to 6 by the addition of HCl. Samples were prepared by adding 10 mL of the Laponite dispersion into an adequate volume of the macroRAFT and completed with water until a total volume of 40 mL (in order to obtain a 5 g L^{-1} dispersion of Laponite containing different concentrations of macroRAFT agent). The concentration of macroRAFT agent in the final dispersion was selected based on the adsorption isotherm of this macroRAFT agent (**Error! Reference source not found.**5) and the evolution of Zeta potential. Therefore, four concentrations were analyzed, as listed below:

- Pure Laponite RD (after being submitted to the dispersion procedure);
- Dispersion of Laponite (5 g L^{-1}) and 0.2 mM of P(DMAEMA$_{19}$-*co*-BA$_{14}$)-CTPPA (this point is below the point of charge inversion of macroRAFT-modified Laponite platelets);

– Dispersion of Laponite (5 g L^{-1}) and 0.6 mM P(DMAEMA$_{19}$-*co*-BA$_{14}$)-CTPPA (this point is above the point of charge inversion of macroRAFT-modified Laponite platelets and there is no free macroRAFT agent in the aqueous phase);

– Dispersion of Laponite (5 g L^{-1}) and 1.5 mM of P(DMAEMA$_{19}$-*co*-BA$_{14}$)-CTPPA (this point is above the point of charge inversion of macroRAFT-modified Laponite platelets and there is an excess of macroRAFT agent that is free in the aqueous phase).

XRD results are shown in **Figure S9**.

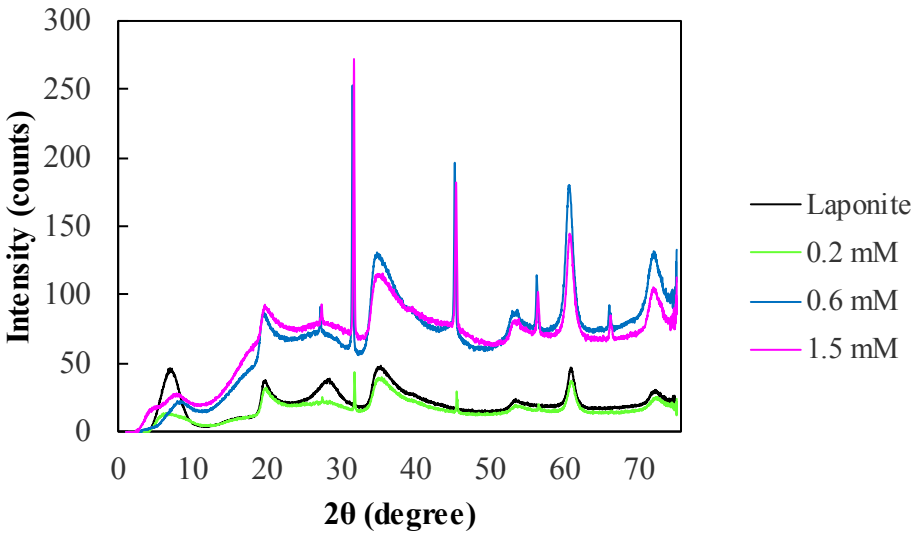

Figure S9. XRD analysis of Laponite (5 g L^{-1}) modified with different concentrations of P(DMAEMA$_{19}$-*co*-BA$_{14}$)-CTPPA macroRAFT agent at pH 6.

The XRD pattern of Laponite in the sodium cation form presents a broad peak at about 6.9º (2θ) associated to a (001) basal spacing of ~ 0.79 nm. At low macroRAFT concentration (0.2 mM), a peak of lower intensity is observed at 6.4º (2θ), which can be associated to a basal spacing of ~ 0.77 nm. This means that, at low concentration of macroRAFT, the basal spacing of the mineral does not suffer a significant change. Confirming the close interaction between the clay platelets and P(DMAEMA$_{19}$-*co*-BA$_{14}$)-CTPPA chains at a concentration of 0.6 mM of macroRAFT, a small peak can be noticed around 7.9º (2θ) associated to a Laponite basal spacing of 0.88 nm. This expansion in the basal spacing after contact with 0.6 mM of DMAEMA-based copolymer suggests the intercalation of the polymer chains. Increasing the concentration of macroRAFT to 1.5 mM does not affect the basal spacing of Laponite, as very similar results were obtained at this concentration (2θ = 7.8 º with a basal spacing of 0.87 nm), indicating that the excess of macroRAFT does not intercalate but stays free in the aqueous phase.

REFERENCES

(1) Langmuir, I. The adsorption of gases on plane surfaces of glass, mica and platinum. *J. Am. Chem. Soc.* **1918,** *40*, 1361-1403.
(2) Freundlich, H. Concerning adsorption in solutions. *Z. Phys. Chem.* **1906,** *57* (4), 385-470.
(3) Sips, R. On the Structure of a Catalyst Surface. *J. Chem. Phys.* **1948,** *16* (5), 490-495.
(4) Redlich, O.; Peterson, D. L. A Useful Adsorption Isotherm. *J. Phys. Chem.* **1959,** *63* (6), 1024-1024.

(5) Brunauer, S.; Emmett, P. H.; Teller, E. Adsorption of Gases in Multimolecular Layers. *J. Am. Chem. Soc.* **1938,** *60* (2), 309-319.
(6) Ebadi, A.; Soltan Mohammadzadeh, J. S.; Khudiev, A. What is the correct form of BET isotherm for modeling liquid phase adsorption? *Adsorption* **2009,** *15* (1), 65-73.
(7) Bourgeat-Lami, E.; França, A. J. P. G.; Chaparro, T. C.; Silva, R. D.; Dugas, P. Y.; Alves, G. M.; Santos, A. M. Synthesis of Polymer/Silica Hybrid Latexes by Surfactant-Free RAFT-Mediated Emulsion Polymerization. *Macromolecules* **2016,** *49* (12), 4431-4440.
(8) Silva, R. D.; Stefanichen Monteiro, I.; Chaparro, T. d. C.; Silva Hardt, R.; Giudici, R.; Barros-Timmons, A.; Bourgeat-Lami, E.; Martins dos Santos, A. Investigation of the Adsorption of Amphipathic macroRAFT Agents onto Montmorillonite Clay. *Langmuir* **2017,** *33* (38), 9598-9608.